Local host response of commercially available dural patches for fetal repair of spina bifida aperta in rabbit model

Yada Kunpalin[a,b], Simen Vergote[a,c], Luc Joyeux[d,*], Onur Telli[a], Anna L David[a,b], Michael Belfort[d], Paolo De Coppi[a,f], Jan Deprest[a,b,c,f]

[a] MyFetUZ Fetal Research Center, Department of Development and Regeneration, Cluster Woman and Child, Biomedical Sciences, KU Leuven, Leuven, Belgium

[b] Elizabeth Garrett Anderson Institute for Women's Health, University College London, UK

[c] Department of Obstetrics and Gynaecology, University Hospitals Leuven, Leuven, Belgium

[d] Division of Pediatric Surgery, Texas Children's Hospital and Michael E. DeBakey Department of Surgery, Baylor College of Medicine, Houston, Texas, USA

[f] Great Ormond Street Institute of Child Health, University College London, UK

Short title: Fetal spina bifida closure with dural patch conserves motor neuron density of the spinal cord in fetal rabbit model

Corresponding author:

Jan Deprest

Department of Development and Regeneration,

Biomedical Sciences, KU Leuven, Leuven, Belgium

Email: Jan.deprest@uzleuven.be

Number of Tables: 1

Number of Figures: 4

Word count: 4124

Keywords: neural tube defects, spina bifida aperta, myeloschisis, Arnold-Chiari II malformation, dural patch, fetal surgery

This article has been accepted for publication and undergone full peer review but has not been through the copyediting, typesetting, pagination and proofreading process, which may lead to differences between this version and the Version of Record. Please cite this article as doi: 10.1002/pd.6315.

What is known?

- Fetal spina bifida repair improves outcome as compared to postnatal repair.
- The standard clinical neurosurgical technique is a layered watertight closure using native tissues.
- Most fetoscopic techniques use a commercially available dural patch to cover the spinal cord, but the experimental basis for this is limited.

What is new?

- In the fetal spina bifida rabbit model, two-layer repair using commercially available dural patch and skin closure, conserves motor neuron density and reduces inflammation in the fetal spinal cord.

Abstract (200 words)

Objective: Fetal surgery for spina bifida aperta (SBA) by open hysterotomy typically repairs anatomical native tissue in layers. Increasingly, fetoscopic repair is performed, using a dural patch followed by skin closure. We studied the host response to selected-commercially available patches currently being used, in a fetal rabbit model for spina bifida repair.

Methods: SBA was surgically induced at 23-24 days of gestation (term=31d). Fetal rabbits were assigned to unrepaired (SBA group), or immediate repair with Duragen™ or Durepair™. Non-operated littermates served as normal controls. At term, spinal cords underwent immunohistochemical staining including Nissl and GFAP. We hypothesized that spinal cord coverage with a dural patch and skin closure would preserve motor neuron density within the non-inferiority limit of 201.65 cells/mm^2, and reduce inflammation compared to unrepaired SBA fetuses.

Results: Motor neuron density assessed by Nissl staining was conserved both by Duragen (n=6, 89.5; 95%CI -158.3 to-20.6) and Durepair (n=6, 37.0; 95%CI -132.6 to-58.5), whereas density of GFAP-positive cells to quantify inflammation was lower than in unrepaired SBA-fetuses (SBA 2366.0±669.7 cells/mm^2 vs Duragen 1274.0±157.2 cells/mm^2;p=0.0002, Durepair 1069.0±270.7cells/mm^2;p<0.0001).

Conclusions: Covering the rabbit spinal cord with either Duragen or Durepair followed by skin closure, preserves motor neuron density and reduces the inflammatory response.

Introduction

Spina bifida aperta (SBA) is a severe congenital malformation of the central nervous system with a prevalence of 2-6 cases per 10,000 live births (1). The malformation stems from an incomplete closure of the neural tube during the third to the fourth week of embryonic development (2). The defect in the vertebrae and the overlying tissues allows direct mechanical and chemical trauma from the intra-uterine environment to the non-neurulated neural placode. This eventually leads to significant, lifelong spinal cord dysfunction including lower limb sensorimotor impairment, bowel and bladder dysfunction, and in some cases orthopaedic complications (3). There is overwhelming evidence in both animal models as well as clinical studies that the injury to the uncovered placode is progressive throughout gestation. Therefore, *in-utero* closure of the defect should arrest this process (4-6). Following animal and early clinical studies, the Management of Myelomeningocele Study (MOMS) trial provided level-I evidence that prenatal repair preserves motor function and reduces the need of postnatal ventriculoperitoneal shunt placement. Fetuses with SBA who were operated before birth were less likely to require a shunt at one year of age, and had better lower limb motor function at 2.5 years, when compared to individuals who were operated after birth (7, 8). Follow-up studies in the MOMS2 trial demonstrated that these benefits persist into the school age (9).

Fetal surgery comes at a price of several fetal and maternal complications including, but not limited to chorioamniotic separation, fetal membrane rupture, preterm delivery, uterine dehiscence and/or rupture, the latter even beyond the index pregnancy (7, 10) (11). The MOMS trial used an open fetal surgery technique with a hysterotomy scar of 6-8cm. Lesser invasive surgical methods through mini-hysterotomy (scar <4cm) or fetoscopy are therefore being explored (12, 13). Most fetoscopic techniques do not exactly mimic the neurosurgical procedure done by the open hysterotomy technique. The latter is a multi-layered anatomical closure using mostly native tissues including dura (if possible), myofascial flaps and skin (7). In comparison, most fetoscopic techniques insert a dural patch over the spinal cord, to simplify the techniques and to achieve a watertight repair (14). To our knowledge, there is only one biocellulose patch which was experimentally tested for fetal SBA repair in a fetal rabbit model (Biofill®, Fibrocel, Parana, Brazil)(15, 16). Other more widely available dural patches used in adult neurosurgery, such as the DuraGen® Plus™ (Integra, New Jersey, USA)

and Durepair™ Regeneration Matrix (Medtronic, Minneapolis, USA), have not been formally tested for fetal surgery, although they are already used clinically (7, 17). Herein we aimed to determine the local effects of these patches on the growing spinal cord of a fetal rabbit at the time of simulated SBA repair, so that the findings from this study can be later used as a benchmark for other dural patches.

Material and methods

This experiment was approved by the Ethics Committee for Animal Experimentation of the Faculty of Medicine, KU Leuven (P202/2018 and P032/2021). Experiments were treated according to NC3R2 (National Center for the Replacement, Refinement, and Reduction of Animals in Research) and ARRIVE (Animals in Research Reporting *In Vivo* Experiments) guidelines for animal well-being (18, 19) .

Study design

The host local immune response to the patches was studied previously in an established surgically induced SBA model in the fetal rabbit (20-22). Because of the paucity of published information and our lack of experience with the model and the readouts, the first batch of the animals were employed to document the effect of an unrepaired SBA defect on the spinal cord and to compare findings with those in healthy littermates of the same pregnancy ('normal controls', n=6). Based on the observations in pups with an unrepaired SBA lesion, we performed a power calculation for the neuron density as measured by Nissl staining, in the anterior horn compared to that of normal control pups. Our hypothesis was that immediate fetal SBA repair i.e. coverage with dural patches and primary skin closure, should conserve the neuronal density within the range of that observed in the normal controls. Additionally, we calculated the sample size needed to demonstrate that the surgically patch-repaired groups displayed a lower local inflammatory response than those with an unrepaired SBA lesion. Inflammation was measured by the density of glial fibrillary acidic protein (GFAP)-positive cells and their occupied area in operated SBA fetuses, compared to the unrepaired SBA fetuses (Supplementary Information 1).

For the second batch of animals, a block-of-four randomisation was performed to allocate pups to either one of the two immediately repaired groups; repair with DuraGen® Plus™ Adhesion Barrier Matrix (Integra, New Jersey, USA); further referred to as "DuraGen" or Durepair™ Regeneration Matrix (Medtronic, Minneapolis, USA); further referred to as "Durepair".

Experimental procedure

Time-mated pregnant rabbit does (hybrid of Dendermonde and New Zealand White) were housed in separate cages at 21°C, 42% humidity, with a 12-hour day-night cycle and free

access to water and food. Animals were housed for approximately three day before the surgery to allow acclimatisation.

SBA induction

Induction of an SBA defect was performed at 23-24 days gestation (term=31 d) by the following surgical steps. Does were premedicated with ketamine (35 mg/kg IM; Nimatek® 100 mg/ml, Dechra, Northwich, UK) and Xylazine (5 mg/kg IM; Xyl-M® 20 mg/ml, V.M.D. nv/sa, Groningen, Netherlands). After premedication, general anaesthesia was achieved with an inhaled oxygen/isoflurane (0.8-1.5%) mixture delivered via facemask. The doe was allowed to breath spontaneously throughout the procedure and was monitored with pulse oximetry. Intravenous access was placed in the ear and maintained with warm fluid replacement (Plasma-Lyte; Baxter, Illinois, USA) at a rate of 10 mL/kg/hr. Buprenorphine (0.05 mg/kg; Vetergesic® 0.3 mg/mL, CEVA, Libourne, France), Enrofloxacin (10 mg/kg, Baytril® 25 mg/mL, Bayer, Leverkusen, Germany) and medroxyprogesterone acetate (Depo-Provera® 150 mg/mL, Pfizer, New York, USA) were given subcutaneously.

The doe was positioned supine on a heating pad, then the abdomen was shaved, prepped with iodine solution, and covered with sterile drapes. A low midline laparotomy (approximately 5 cm) was performed to partially expose the bicornuate uterus. Up to two cornual end fetuses were operated under a 3.5X loupe magnification. Only the targeted gestation sac involved in the surgery was exteriorized and surrounded by a gauze soaked in warm saline. The fetus was palpated and adjusted to a suitable position for surgery. A 1.5-cm diameter purse string suture was placed through the myometrium and membranes on the antimesenteric side of the uterus, above the fetal back using polypropylene 6/0 (Prolene, Ethicon, New Jersey, USA) before performing a 1-cm linear hysterotomy in the middle of the purse string. Chorionic and amniotic membranes were sharply dissected to enter the amniotic cavity. The lower part of the fetus from the tail was gently exteriorised up to its lower lumbar region (Fig 1B). A 1-cm diameter circular skin defect was created over the lumbar spine beginning at the level of the posterior iliac crest. Bilateral paraspinal muscles were removed over the area of 3-lumbar vertebral bodies. A laminectomy and durectomy with a sharp 26G needle (BD Microlance™ 3, BD, New Jersey, USA) were done until confirmation of CSF leakage. In this model no myelotomy was performed, in other words the central canal was not opened (20). In the unrepaired SBA group, there were no further fetal manipulations.

The fetus was returned to the uterus, amniotic fluid (AF) volume was restored with warmed saline. The purse string suture was tied closing the hysterotomy site and another imbricated interrupted suture was placed on top with polypropylene 6/0 (Prolene, Ethicon, New Jersey, USA) to prevent any amniotic fluid leakage. The doe's abdominal wall fascia was closed with continuous PDS*II 2/0 (Ethicon, New Jersey, USA). The subcutaneous layer and the skin was approximated with Monocryl 3/0 (Ethicon, New Jersey, USA). The doe was given 4 mL of local anaesthesia at the incision site (levobupivacaine; Chirocaine 5 mg/mL, Fresenius Kabi, Bad Homburg, Germany) and buprenorphine for analgesia (0.03 mg/kg SC; Vetergesic® 0.3 mg/mL, CEVA, Libourne, France) upon awakening and every 12 hours for 48 hours. Rabbits were monitored daily using the Rabbit Grimace Scale (23).

Surgical SBA repair

For the pups allocated to undergo an immediate repair with either Duragen or Durepair, the skin around the defect was undermined to avoid any tension or tearing that may occur during the closure. A 1-cm diameter patch was applied on the spinal cord and fixed with 4 stay sutures (PDS*II 6/0; Ethicon, New Jersey, USA) to the paraspinal muscle and fascia. Finally, the skin was closed over the patch by a running suture (PDS*II 6/0; Ethicon, New Jersey, USA).

Harvesting

Near term (30-31 d), the does underwent terminal caesarean delivery. Prior to euthanasia, animals were sedated as previously described with an intravenous bolus of pentobarbital (1 mL Euthasol® vet 400 mg/mL, Dechra, Northwich, UK). The interval between euthanasia and delivery was kept between 15-20 minutes. Fetuses were harvested, weighed and measured, including the length and width of the defect, and in the fetuses who underwent prenatal repair, the length of the scar was measured and CSF leakage was determined by blotting paper (Easy V2 White, Lucart Professional, Diecimo, Italy) (15).

Pathology

The fetal lumbar spine, as well as the head and cervical spine were dissected en bloc and fixed in 4% formaldehyde (Klinipath BV, Olen, Netherlands) in 0.1 mol/L phosphate buffer (pH 7.4) for at least 72 hours. The head and cervical spine were sharply dissected across the sagittal plane. To evaluate for hindbrain herniation (HH) as an indicator for adequate SBA creation, a Basion-to-Opisthion line was arbitrarily drawn as a reference for the margin of foramen

magnum. HH was classified if the position of cerebellar tonsil descended below the reference line (24).

The lumbar spine tissue was dehydrated in gradient ethanol solutions (70.0-99.9%) ended with 100% technical toluene (VWR Chemicals) before embedding in paraffin blocks. For each pup, the central level of the defect was serially sectioned at 4 μm with an interval of 100 μm (4 cross-sections/sample) on an automated microtome (Epredia™ HM 355S, Fisher Scientific, Massachusetts, USA). Following sectioning, haematoxylin and eosin (H&E) and Nissl (cresyl violet) staining was performed. For immunostaining with glial fibrillary acidic protein (GFAP), paraffin sections were de-paraffinized and rehydrated in technical toluene followed by gradient ethanol solutions before rinsing in 0.01M tris-buffered saline (TBS, pH7.6). Sections were then blocked with 3% hydrogen peroxide (Millipore, Massachusetts, USA) in 0.01M TBS for 30 mins at room temperature (RT) and washed with 0.01M TBS. After that, sections were incubated in 0.01M TBS containing 0.1% Tween 80, 2% bovine serum albumin (BSA) and 1% non-fat dry milk for 1 hour at RT. Sections were incubated with monoclonal mouse antibody against GFAP (1 μg/ml; cat no. G6171, Sigma-Aldrich, Missouri, USA) overnight at 4 °C. Antibodies were washed with 0.01M TBS and again blocked with 0.1% Tween 80, 2% BSA and 1% non-fat dry milk for 15 mins at room temperature before adding peroxide (PO)-conjugated secondary goat antibody against mouse IgG and IgM (cat no. 115-035-044, Jackson ImmunoResearch, Pennsylvania, USA) and 4% rabbit serum (DAKO, Glostrup, Denmark) for 30 mins at RT. The PO conjugation was reacted in a 0.01M TBS solution containing di-aminobenzidine (DAB, 0.5 mg/ml) and 0.1% hydrogen peroxide for 10 mins at RT. Nuclei were stained with Mayer's haematoxylin solution. Following nuclear staining, sections were rinsed with tap water and distilled water, dehydrated in gradient ethanol solutions and Neo-Mount® (Millipore, Massachusetts, USA) and sealed with Neo-clear® (Millipore, Massachusetts, USA).

Slides were scanned with a microscope slide scanner (Axioscan Z1, Zeiss, Oberkochen, Germany) to obtain digital images before analysing with QuPath software (25). On each slide of H&E staining, total cross-sectional area, grey matter area (total and anterior horn) and white matter area of the spinal cord were determined. Motor neurons defined by a Nissl stained cell with a diameter of 30-70 μm and a discernible nucleolus, GFAP-positive cells and its fibre in the anterior horn of the grey matter, were semi-automatically counted and quantified from the digital image (x20 magnification) (26-28). Motor neuron density, GFAP

glial cell density and its fibre density were calculated by dividing the number of motor neurons, GFAP glial cells or the area of GFAP-positive fibre (mm^2) by mm^2 of grey matter, respectively.

Statistical analysis

To declare non-inferiority for motor neuron density, the lower boundary of the 95% confidence interval (CI) of the pups undergoing immediate SBA repair with dural patches, must lie above the non-inferiority margin (Δ) limit (29). We did not perform a non-inferiority analysis for the inflammatory response as we expected that any surgery related to the spinal cord would induce a local reaction. We applied superiority analysis to determine inflammatory responses represented by GFAP cells and its fibres. In this case, we wanted to demonstrate that the incorporation of a dural patch would reduce the inflammatory response when compared to the unrepaired SBA lesion. Thus, this analysis compared the immediate SBA repair groups to the unrepaired SBA group. For superiority analysis, one-way analysis of variance (ANOVA) with Dunnett correction for post hoc analysis was used for continuous variables and Pearson's chi-squared test with Bonferroni correction was applied for categorical variables. Statistical analysis was carried out by GraphPad Prism software version 9.0.0 (California, USA). A p-value of <0.05 was considered statistically significant and data is presented as mean ± SD.

Results

Demographic data

Fourteen pups from eight does underwent surgical induction of SBA (unrepaired group). Thirty-three pups in another 18 does underwent SBA induction followed by immediate surgical repair, either using Duragen (n=16) or Durepair (n=17). Survival rate in the unrepaired group was 57.1% (8/14), which was comparable to the repaired SBA groups (50% (8/16) with Duragen and 41.2% (7/17) with Durepair) (Table 1). Birth weights of both of the repaired SBA groups were no different to normal controls (Table 1). However, birthweight of the unrepaired SBA fetuses were significantly less than that of the normal controls (controls; 49.2±4.2 gm vs SBA fetuses 41.4±4.5 gm, p=0.03). Two pups from the Duragen group and one from the Durepair group were born with apparent wound dehiscence and persistent CSF leakage (Duragen 25.0% (2/8) vs Durepair 12.5% (1/7), p>0.99). These pups displayed hindbrain herniation at necropsy, similar to what was seen in nearly all of the pups in the unrepaired SBA group (87.5% (7/8)) (Fig 1e). The repaired SBA pups with wound dehiscence were excluded from the histological analysis. Pups with successful SBA repair (no CSF leakage) did not display any hindbrain herniation. Macroscopic adhesion between spinal cord and dural patch was identified in 50% (4/8) of the Duragen group. The adhesion was sparse and easily removed without sharp dissection. On the contrary, none were noted in the Durepair group.

Spinal cord structure analysis

Histology of the spinal cord confirmed an SBA-like lesion in the unrepaired group. The spinal cord showed an extensive degree of damage, in particular in the posterior horn where it was nearly or completely lost, whereas the anterior horn remained recognizable but was smaller in size. Spinal cords of fetuses in the repaired SBA groups were well preserved (Fig 2).

Quantification of several selected areas of the spinal cord confirmed the above macroscopic findings. Unrepaired SBA fetuses had a significantly smaller total surface area and the area of grey matter on transection, when compared to the normal controls or fetuses with immediate SBA repair (total spinal cord area; unrepaired SBA 0.81±0.46 mm^2 vs control 2.35±0.42 mm^2, Duragen 2.35±0.48 mm^2, Durepair 2.25±0.19 mm^2; all p<0.0001 when compared to the unrepaired SBA group) (grey matter area; unrepaired SBA 0.46±0.22 mm^2 vs control

1.55±0.25 mm^2, Duragen 1.69±0.13 mm^2, Durepair 1.51±0.21 mm^2; all p<0.0001 when compared to the unrepaired SBA group). Interestingly, the fetuses in the unrepaired SBA group had a significantly smaller anterior horn, compared to the other groups (unrepaired SBA 0.30±0.14 mm^2 vs control 0.59±0.12 mm^2; p=0.005, Duragen 0.59±0.18 mm^2; p=0.006, Durepair 0.53±0.05 mm^2; p=0.03) (Fig 2). The loss of the posterior horn in the unrepaired SBA fetuses made the area of the anterior horn dominant, hence it occupied half of the whole area of the grey matter. This was significantly more than in the other groups (unrepaired SBA 50.61±4.91% vs control 32.05±2.91%, Duragen 31.61±2.60%, Durepair 29.03±3.85%; all p<0.0001 when compared to the unrepaired SBA group) (Fig 2).

In conclusion, the creation of an SBA defect in fetal rabbits at 23-24 gestational days, resulted in a homogenous phenotype of SBA-like spinal cord injury by (near) term gestation. Immediate repair of the SBA lesion with dural patches and skin approximation preserved the structure of the spinal cord.

Motor neuron density

When examining the anterior horn of the spinal cord, pups with unrepaired SBA lesions had a significantly lower motor neuron density when compared to the controls control pups had significantly higher motor neuron density when compared to the unrepaired SBA group (830.80±71.81 cells/mm^2 vs 383.0±42.38 cells/mm^2; p<0.0001) (fig 3b). In the repaired SBA groups, the means and SDs of motor neuron density in the Duragen and the Durepair groups were 741.30±65.60 cells/mm^2 and 793.80±91.06, respectively. To determine whether the motor neuron density in fetuses of the Duragen and Durepair groups were not inferior to that of the normal controls, a non-inferiority analysis was performed. The analysis showed that the 95%CIs of the difference between the patch-repaired SBA groups and the normal controls lay within the predefined Δ limit (Duragen -89.5 (95%CI -158.3 to -20.6) and Durepair 37.0 (95%CI -132.6 to -58.5) as shown in figure 3c. This confirmed the non-inferiority for the motor neuron density in both the patch-repaired SBA groups.

GFAP-positive cell and their area

The density of GFAP-positive cells in the anterior horn of the spinal cord was significantly higher in the unrepaired SBA fetuses when compared to any of the other groups (unrepaired SBA 2366.0±669.7 cells/mm^2 vs control 687.6±125.5 cells/mm^2; p<0.0001, Duragen

1274.0±157.2 cells/mm^2; p=0.0002, Durepair 1069.0±270.7 cells/mm^2; p<0.0001) (Fig 4b). The same difference was observed with the percentage of the area of GFAP positive fibres relative to the area of the anterior horn (unrepaired SBA 35.87±9.52% vs control 9.82±2.94%; p<0.0001, Duragen 18.05±6.08%; p=0.0002, Durepair 19.19±4.01%; p=0.0004).

Discussion

Herein we documented the local host response to commercially available dural patches, DuraGen® Plus™ and Durepair™ Regeneration Matrix in the fetal rabbit SBA model. Similar to clinical fetoscopic procedures, these patches were used to cover an SBA defect followed by a primary skin suture. We quantified the subsequent host response at term by measuring the densities of motor neuron, GFAP positive cells and its area, as proxies for neuroprotection and neuroinflammation, respectively. In the repaired SBA group, the spinal cord of animals without CSF leakage showed at birth no difference in the motor neuron density compared to the normal controls. In other words, there were no histologic signs of motor neurodegeneration, which in contrast, were observed in SBA animals that did not undergo fetal repair. Also, even though fetal repair with patched augmentation induced a local neuroinflammatory response, the inflammation was much less than that observed in the unrepaired SBA group.

This experiment was undertaken to, first, provide experimental data on the safety of these patches when used in the context of fetal surgery. In this model, the surgical SBA defect was induced at 23-24 d of gestation (term=31), and immediately repaired, as previously described (20-22). The timeframe of the simulated fetal SBA repair corresponds to the late second trimester in human gestation. This is obviously not the time point when SBA lesion occurs, it is however the time period when fetal surgery would be performed. In other words, this experiment simulates the local host response following the neurosurgical repair, but not to the pathophysiology of SBA, which occurs much earlier in gestation. Despite these differences with the clinical situation, our findings are relevant as a benchmark for further investigation of alternative covering techniques/devices for fetal repair (30, 31).

Our findings only apply to a specific layered anatomical closure coverage of the spinal cord. This technique is used clinically for fetoscopic repair with the purpose of arresting CSF leakage (14, 32, 33). The multi-layered closure included dural coverage with dural patch followed by skin approximation, but without myofascial or paraspinal muscle closure – which is not possible in this model. The experiment was not designed to compare different neurosurgical techniques, but to determine the difference in local host response to of different dural patches. We excluded animals that displayed any signs of insufficient or non-watertight closure, as unsuccessful closure may be less neuroprotective (14). The experiment was

neither powered to study the spectrum of effects of incomplete SBA closure. Data from incomplete closure were not considered for analysis as experiments in large animal models demonstrate that ongoing leakage is associated with deterioration of hindlimb motor function, hence it is likely to be less neuroprotective (14).

Without surgical repair, fetal rabbits uniformly exhibit an apparent skin defect with protruding spinal cord at birth, similar to what was described by Housley et al and Pedreira et al (20, 21). Of note, the unrepaired SBA lesion at birth is substantially larger than the original defect. We observed that fetal rabbits with evident CSF-leakage also displayed hindbrain herniation (Figure 1E), as previously documented in another experiment by Fontecha et al by histology of an en bloc specimen of the fetal head and cervical column (24). We further observed histological signs of spinal cord damage, in particular in the posterior horn. This is similar to what is observed in human fetuses with SBA as well as in other animal models (6, 34-37).

Compared to earlier experiments (20-22), we refined the readouts, to better document the local host response in the spinal cord. We documented the densities of motor neurons and inflammatory cells by Nissl staining and GFAP immunostaining. Preservation of motor function is considered to be one of the primary advantages of successful fetal SBA surgery (7). A positive correlation between clinical function and motor neuron density was previously demonstrated in several animal studies (38-40). Inflammation is a naturally occurring process to trauma and repair processes. In the case of SBA, excessive neuroinflammation or astrogliosis has been well documented in both the exposed neural placode and its adjacent transitional zone (41-43). Recent evidence shows that the reaction is progressive, resulting in a persistent chronic inflammatory state, which is subsequently detrimental to neuronal survival and repair (37, 42). Therefore, we included quantification of the inflammatory reaction in our analysis of the host response and hypothesized that fetal repair would reduce the inflammatory response, when compared to the unrepaired spinal cord of SBA fetuses.

Currently, there is only one patch, which is specifically tested for fetal SBA surgery, i.e. a biocellulose patch (Biofill®, Fibrocel, Parana, Brazil and Bionext®, Bionest, Parana, Brazil) (15). However, the patch was designed for external use as a wound dressing. Lapa et al tested the patch in fetal rabbit and sheep models before applying it clinically for fetoscopic SBA surgery (16, 22, 44-46). In her initial study in the rabbit model, the repaired defect healed completely,

with the patch remaining in place, and "without any signs of tissue rejection" at term (22). We documented similar effects with both Duragen and Durepair in the same model she used. However, we could not directly compare the dural patches to the biocellulose patch as it was not included in our study. Both the patches are dural substitutes used to cover dural defects and prevent CSF leakage in adult cranial and spinal surgical procedures (47-49). Both are bovine porous decellularized collagen scaffolds that promote neovascularisation and fibroblast infiltration (50, 51). In their typical use, rapid collagen deposition takes place, and within a few weeks, a neodural membrane is formed which should close the dural defect (50, 51).

The main strength of our study is its comprehensive set of readouts, incorporating gross and microscopic analysis of the defect, inflammatory response, neuronal density in the spinal cord and hindbrain herniation. The advantages of rabbits include their short gestation, a higher number of fetuses and lower housing needs than the sheep model, making it an ideal model for surgical experiments, such as the testing of novel dural patches. The model, unfortunately, also has its limitations. These include the need for delicate surgical skills and the high fetal mortality rates. The short interval between the surgery and sacrifice, the size of the animal and our necropsy method may not be optimal for assessing adhesion formation. However, our necropsy method was chosen for optimal preservation of the spinal cord. Other weaknesses are the lack of mid- to long-term outcomes; for example, radiologic findings on tethering cord and epidermal inclusion cyst formation. Lastly, the model does not mimic the natural history of the condition, as the lesion is induced and immediately repaired, so no damage is accumulated prior to the fetal repair.

In conclusion, we demonstrated that DuraGen® Plus™ or Durepair™ Regeneration Matrix preserves motor neuron density in the fetal rabbit model for SBA. Both patches induce a mild inflammatory response in the spinal cord, which is much less than what is observed in fetuses with an unrepaired SBA lesion. Both the dural patches seem to be safe in a fetal environment. We will use findings from this model as a benchmark and screening model for alternative dural patches, prior to their testing in larger models to evaluate for chronic inflammation, fibrosis and cord tethering.

Acknowledgement

We are very grateful for Yannick Regin from Translational cell and tissue research, KU Leuven, for his help during the surgery, Dr. David Basurto and Dr. Ignacio Valenzuela. We also thank the following Katrien Luyten and Sofie Jannes of the G-PURE laboratory for their technical support.

Statement of Ethics

This study protocol was reviewed and approved by the Ethics Committee for Animal Experimentation of the Faculty of Medicine, Katholieke Universiteit Leuven (P202/2018 and P032/2021). Experiments were treated according to NC3R2 (National Center for the Replacement, Refinement, and Reduction of Animals in Research) and ARRIVE (Animals in Research Reporting *In Vivo* Experiments) guidelines for animal well-being

Conflict of Interest Statement

DuraGen® Plus™ patches used in this study are supported by Integra LifeSciences Corporation, Boston, Massachusetts, USA.

Funding sources

YK is supported through an Innovative Engineering for Health award by the Wellcome Trust (WT101957), an Engineering and Physical Sciences Research Council (EPSRC)(NS/A000027/1) and the UCL Overseas Research Scholarship.

SV is supported by the Flanders Research Foundation (Fonds Wetenschappelijk Onderzoek Vlaanderen T002618N).

LJ is supported by an Innovative Engineering for Health award by the Wellcome Trust (WT101957) and the Engineering and Physical Sciences Research Council (EPSRC) (NS/A000027/1)

PDC is supported by the National Institute for Health Research (NIHRRP-2014-04-046) and the NIHR BRC at GOSH

ALD is supported by by the National Institute for Health Research (NIHR) University College London Hospitals Biomedical Research Centre (BRC).

JDP is a clinical researcher of the FWO (FWO-1.8.012.07) and is also supported by the Great Ormond Street Hospital Children's Charity.

Author contributions

YK: design of the work, acquisition, analysis and interpretation of data and drafting of the work.

LJ: design of the work, acquisition, and clitically revising the manuscript of the work.

SV: acquisition of the data and critically revising the manuscript of the work.

OT: acquisition of the data and critically revising the manuscript of the work.

PDC: design of the work, interpretation of data and critically revising the manuscript of the work.

ALD: design of the work, interpretation of data and critically revising the manuscript of the work.

JD: design of the work, interpretation of data, drafting and critically revising the manuscript of the work.

Data availability Statement

The authors confirm that the data supporting the findings of this study are available within the article [and/or] its supplementary materials.

Reference

1. EUROCAT Guide 1.4. Instructions for the registration and surveillance of congenital anomalies [Online]. [Internet]. 2013 [cited 22 July 2021]. Available from: http://www.eurocat-network.eu/accessprevalencedata/prevalencetables.
2. Greene ND, Copp AJ. Neural tube defects. Annu Rev Neurosci. 2014;37:221-42.
3. Adzick NS. Fetal surgery for spina bifida: past, present, future. Semin Pediatr Surg. 2013;22(1):10-7.
4. Sival DA, Begeer JH, Staal-Schreinemachers AL, Vos-Niel JM, Beekhuis JR, Prechtl HF. Perinatal motor behaviour and neurological outcome in spina bifida aperta. Early Hum Dev. 1997;50(1):27-37.
5. Meuli M, Meuli-Simmen C, Yingling CD, Hutchins GM, Hoffman KM, Harrison MR, et al. Creation of myelomeningocele in utero: a model of functional damage from spinal cord exposure in fetal sheep. J Pediatr Surg. 1995;30(7):1028-32; discussion 32-3.
6. Ben Miled S, Loeuillet L, Duong Van Huyen JP, Bessieres B, Sekour A, Leroy B, et al. Severe and progressive neuronal loss in myelomeningocele begins before 16 weeks of pregnancy. Am J Obstet Gynecol. 2020;223(2):256 e1- e9.
7. Adzick NS, Thom EA, Spong CY, Brock JW, 3rd, Burrows PK, Johnson MP, et al. A randomized trial of prenatal versus postnatal repair of myelomeningocele. N Engl J Med. 2011;364(11):993-1004.
8. Farmer DL, Thom EA, Brock JW, 3rd, Burrows PK, Johnson MP, Howell LJ, et al. The Management of Myelomeningocele Study: full cohort 30-month pediatric outcomes. Am J Obstet Gynecol. 2018;218(2):256 e1- e13.

9. Houtrow AJ, Thom EA, Fletcher JM, Burrows PK, Adzick NS, Thomas NH, et al. Prenatal Repair of Myelomeningocele and School-age Functional Outcomes. Pediatrics. 2020;145(2).
10. Johnson MP, Bennett KA, Rand L, Burrows PK, Thom EA, Howell LJ, et al. The Management of Myelomeningocele Study: obstetrical outcomes and risk factors for obstetrical complications following prenatal surgery. Am J Obstet Gynecol. 2016;215(6):778 e1- e9.
11. Goodnight WH, Bahtiyar O, Bennett KA, Emery SP, Lillegard JB, Fisher A, et al. Subsequent pregnancy outcomes after open maternal-fetal surgery for myelomeningocele. Am J Obstet Gynecol. 2019;220(5):494 e1- e7.
12. Peralta CFA, Botelho RD, Romano ER, Imada V, Lamis F, Junior RR, et al. Fetal open spinal dysraphism repair through a mini-hysterotomy: Influence of gestational age at surgery on the perinatal outcomes and postnatal shunt rates. Prenat Diagn. 2020;40(6):689-97.
13. Sanz Cortes M, Chmait RH, Lapa DA, Belfort MA, Carreras E, Miller JL, et al. Experience of 300 cases of prenatal fetoscopic open spina bifida repair: report of the International Fetoscopic Neural Tube Defect Repair Consortium. Am J Obstet Gynecol. 2021;225(6):678 e1-e11.
14. Joyeux L, van der Merwe J, Aertsen M, Patel PA, Khatoun A, Mori da Cunha M, et al. Neuroprotection is improved by watertightness of fetal spina bifida repair in fetal lamb. Ultrasound Obstet Gynecol. 2022.
15. Lapa Pedreira DA, Acacio GL, Goncalves RT, Sa RAM, Brandt RA, Chmait RH, et al. Percutaneous fetoscopic closure of large open spina bifida using a bilaminar skin substitute. Ultrasound Obstet Gynecol. 2018;52(4):458-66.
16. Sanchez e Oliveira Rde C, Valente PR, Abou-Jamra RC, Araujo A, Saldiva PH, Pedreira DA. Biosynthetic cellulose induces the formation of a neoduramater following pre-natal correction of meningomyelocele in fetal sheep. Acta Cir Bras. 2007;22(3):174-81.
17. Belfort MA, Whitehead WE, Shamshirsaz AA, Espinoza J, Nassr AA, Lee TC, et al. Comparison of two fetoscopic open neural tube defect repair techniques: single- vs three-layer closure. Ultrasound Obstet Gynecol. 2020;56(4):532-40.
18. Burden N, Chapman K, Sewell F, Robinson V. Pioneering better science through the 3Rs: an introduction to the national centre for the replacement, refinement, and reduction of animals in research (NC3Rs). J Am Assoc Lab Anim Sci. 2015;54(2):198-208.
19. Percie du Sert N, Hurst V, Ahluwalia A, Alam S, Avey MT, Baker M, et al. The ARRIVE guidelines 2.0: updated guidelines for reporting animal research. BMJ Open Sci. 2020;4(1):e100115.
20. Housley HT, Graf JL, Lipshultz GS, Calvano CJ, Harrison MR, Farmer DL, et al. Creation of myelomeningocele in the fetal rabbit. Fetal Diagn Ther. 2000;15(5):275-9.
21. Pedreira DA, Valente PR, Abou-Jamra RC, Pelarigo CL, Silva LM, Goldenberg S. A different technique to create a 'myelomeningocele-like' defect in the fetal rabbit. Fetal Diagn Ther. 2002;17(6):372-6.
22. Pedreira DA, Valente PR, Abou-Jamra RC, Pelarigo CL, Silva LM, Goldenberg S. Successful fetal surgery for the repair of a 'myelomeningocele-like' defect created in the fetal rabbit. Fetal Diagn Ther. 2003;18(3):201-6.
23. Keating SC, Thomas AA, Flecknell PA, Leach MC. Evaluation of EMLA cream for preventing pain during tattooing of rabbits: changes in physiological, behavioural and facial expression responses. PLoS One. 2012;7(9):e44437.

24. Fontecha CG, Aguire M, Soldado F, Peiro JL, Toran N, Vidal N, et al. Effects of birth advancement in Chiari malformation in a surgical myelomeningocele model in rabbits. J Pediatr Surg. 2010;45(3):594-9.
25. Bankhead P, Loughrey MB, Fernandez JA, Dombrowski Y, McArt DG, Dunne PD, et al. QuPath: Open source software for digital pathology image analysis. Sci Rep. 2017;7(1):16878.
26. Gensel JC, Tovar CA, Hamers FP, Deibert RJ, Beattie MS, Bresnahan JC. Behavioral and histological characterization of unilateral cervical spinal cord contusion injury in rats. J Neurotrauma. 2006;23(1):36-54.
27. Brown EG, Keller BA, Lankford L, Pivetti CD, Hirose S, Farmer DL, et al. Age Does Matter: A Pilot Comparison of Placenta-Derived Stromal Cells for in utero Repair of Myelomeningocele Using a Lamb Model. Fetal Diagn Ther. 2016;39(3):179-85.
28. Van der Veeken L, Gronlund S, Gerdtsson E, Holmqvist B, Deprest J, Ley D, et al. Long-term neurological effects of neonatal caffeine treatment in a rabbit model of preterm birth. Pediatr Res. 2020;87(6):1011-8.
29. Schumi J, Wittes JT. Through the looking glass: understanding non-inferiority. Trials. 2011;12:106.
30. Mazzone L, Moehrlen U, Ochsenbein-Kolble N, Pontiggia L, Biedermann T, Reichmann E, et al. Bioengineering and in utero transplantation of fetal skin in the sheep model: A crucial step towards clinical application in human fetal spina bifida repair. J Tissue Eng Regen Med. 2020;14(1):58-65.
31. Guilbaud L, Dugas A, Weber M, Deflers C, Lallemant P, Lilin T, et al. In utero treatment of myelomeningocele with allogenic umbilical cord-derived mesenchymal stromal cells in an ovine model. Curr Res Transl Med. 2022;70(1):103314.
32. Heuer GG, Adzick NS, Sutton LN. Fetal myelomeningocele closure: technical considerations. Fetal Diagn Ther. 2015;37(3):166-71.
33. Blumenfeld YJ, Belfort MA. Updates in fetal spina bifida repair. Curr Opin Obstet Gynecol. 2018;30(2):123-9.
34. Danzer E, Schwarz U, Wehrli S, Radu A, Adzick NS, Flake AW. Retinoic acid induced myelomeningocele in fetal rats: characterization by histopathological analysis and magnetic resonance imaging. Exp Neurol. 2005;194(2):467-75.
35. Stiefel D, Copp AJ, Meuli M. Fetal spina bifida in a mouse model: loss of neural function in utero. J Neurosurg. 2007;106(3 Suppl):213-21.
36. Joyeux L, Engels AC, Van Der Merwe J, Aertsen M, Patel PA, Deprez M, et al. Validation of the Fetal Lamb Model of Spina Bifida. Sci Rep. 2019;9(1):9327.
37. Oria M, Figueira RL, Scorletti F, Sbragia L, Owens K, Li Z, et al. CD200-CD200R imbalance correlates with microglia and pro-inflammatory activation in rat spinal cords exposed to amniotic fluid in retinoic acid-induced spina bifida. Sci Rep. 2018;8(1):10638.
38. Kabagambe S, Keller B, Becker J, Goodman L, Pivetti C, Lankford L, et al. Placental mesenchymal stromal cells seeded on clinical grade extracellular matrix improve ambulation in ovine myelomeningocele. J Pediatr Surg. 2017.
39. Vanover M, Pivetti C, Lankford L, Kumar P, Galganski L, Kabagambe S, et al. High density placental mesenchymal stromal cells provide neuronal preservation and improve motor function following in utero treatment of ovine myelomeningocele. J Pediatr Surg. 2019;54(1):75-9.
40. Galganski LA, Kumar P, Vanover MA, Pivetti CD, Anderson JE, Lankford L, et al. In Utero Treatment of Myelomeningocele with Placental Mesenchymal Stromal Cells - Selection of an Optimal Cell Line in Preparation for Clinical Trials. J Pediatr Surg. 2019.

41. George TM, Cummings TJ. The immunohistochemical profile of the myelomeningocele placode: is the placode normal? Pediatr Neurosurg. 2003;39(5):234-9.
42. Reis JL, Correia-Pinto J, Monteiro MP, Hutchins GM. In utero topographic analysis of astrocytes and neuronal cells in the spinal cord of mutant mice with myelomeningocele. J Neurosurg. 2007;106(6 Suppl):472-9.
43. Meuli M, Meuli-Simmen C, Hutchins GM, Seller MJ, Harrison MR, Adzick NS. The spinal cord lesion in human fetuses with myelomeningocele: implications for fetal surgery. J Pediatr Surg. 1997;32(3):448-52.
44. Pedreira DA, Zanon N, Nishikuni K, Moreira de Sa RA, Acacio GL, Chmait RH, et al. Endoscopic surgery for the antenatal treatment of myelomeningocele: the CECAM trial. Am J Obstet Gynecol. 2016;214(1):111 e1- e11.
45. Lapa DA, Chmait RH, Gielchinsky Y, Yamamoto M, Persico N, Santorum M, et al. Percutaneous fetoscopic spina bifida repair: effect on ambulation and need for postnatal cerebrospinal fluid diversion and bladder catheterization. Ultrasound Obstet Gynecol. 2021;58(4):582-9.
46. Herrera SR, Leme RJ, Valente PR, Caldini EG, Saldiva PH, Pedreira DA. Comparison between two surgical techniques for prenatal correction of meningomyelocele in sheep. Einstein (Sao Paulo). 2012;10(4):455-61.
47. Danish SF, Samdani A, Hanna A, Storm P, Sutton L. Experience with acellular human dura and bovine collagen matrix for duraplasty after posterior fossa decompression for Chiari malformations. J Neurosurg. 2006;104(1 Suppl):16-20.
48. Kshettry VR, Lobo B, Lim J, Sade B, Oya S, Lee JH. Evaluation of Non-Watertight Dural Reconstruction with Collagen Matrix Onlay Graft in Posterior Fossa Surgery. J Korean Neurosurg Soc. 2016;59(1):52-7.
49. Bowers CA, Brimley C, Cole C, Gluf W, Schmidt RH. AlloDerm for duraplasty in Chiari malformation: superior outcomes. Acta Neurochir (Wien). 2015;157(3):507-11.
50. Khorasani L, Kapur RP, Lee C, Avellino AM. Histological analysis of DuraGen in a human subject: case report. Clin Neuropathol. 2008;27(5):361-4.
51. Zerris VA, James KS, Roberts JB, Bell E, Heilman CB. Repair of the dura mater with processed collagen devices. J Biomed Mater Res B Appl Biomater. 2007;83(2):580-8.

Table

Table 1. Demographic data

	Control	Unrepaired SBA	Repaired SBA		P-value		
			Duragen (DG)	Durepair (DP)	DG vs SBA	DP vs SBA	DG vs DP
Survival rate (%, n)	100% (6/6)	57.1% (8/14)	50% (8/16)	41.2% (7/17)	ns	ns	ns
Birth weight (grams)[§]	49.2±4.2	41.4±4.5	43.5±7.3	46.9±4.0	ns	ns	ns
Size of the defect (cm^2)[§]	N/A	5.3±1.4	4.3±0.6[¶]	3.9[¶]	N/A	N/A	N/A
Scar length (cm)[§]	N/A	N/A	1.8±0.3*	1.8±0.4*	N/A	N/A	ns
CSF leakage (%, n)	0% (6/6)	100% (8/8)	25% (2/8)	12.5% (1/7)	0.02	0.004	ns
Hindbrain herniation (%, n)	0% (6/6)	87.5% (7/8)	25% (2/8)	12.5% (1/7)	0.08	0.03	ns

SBA; Spina bifida aperta, DG; Duragen, DP; Durepair, ns; not significant (p>0.05), N/A: not available, [¶]data from two and one animals in Duragen and Durepair groups that had wound dehiscence, respectively, *data from six animals from Duragen and Durepair groups that had intact wound, [§]data presented as mean±SD.

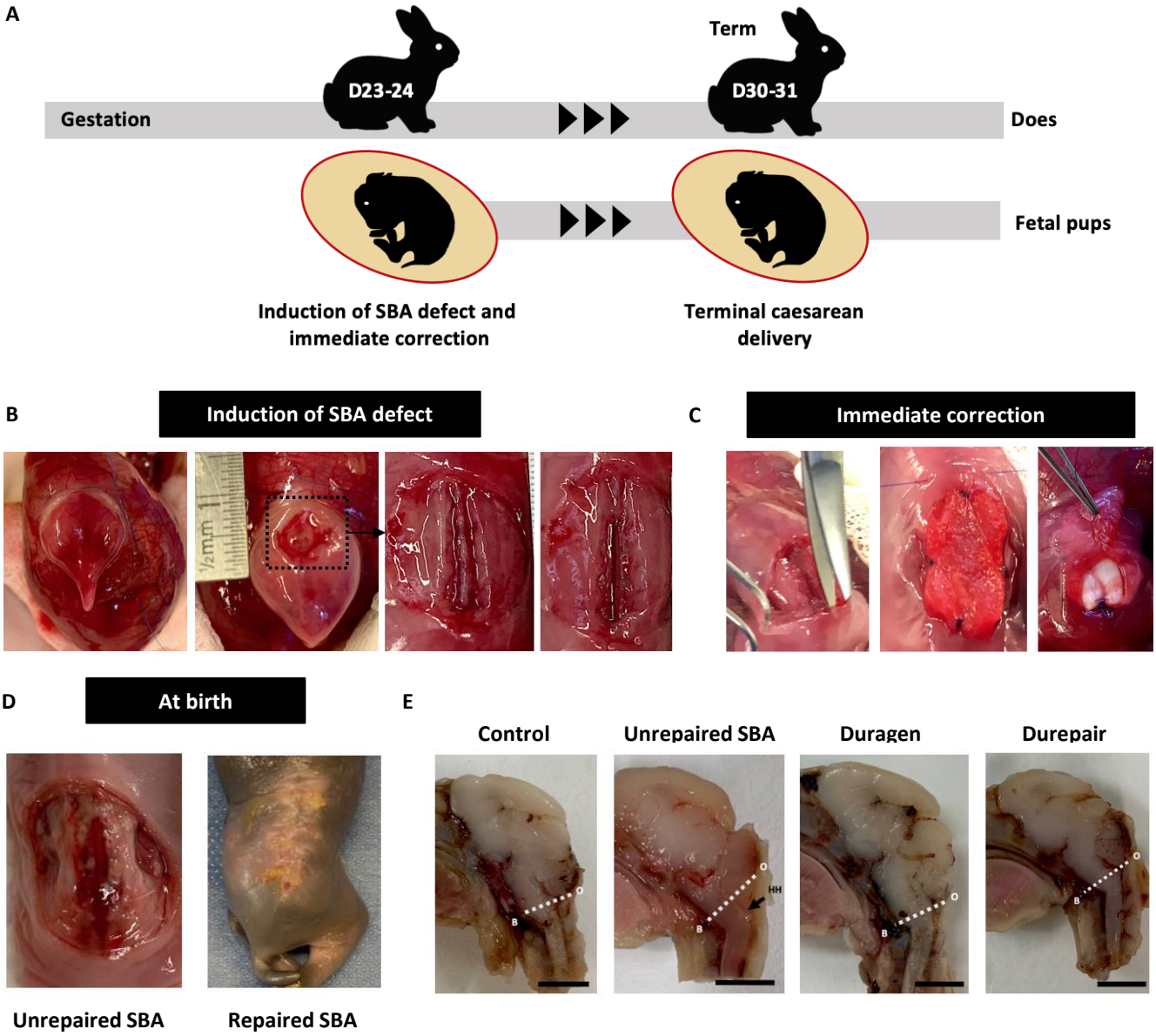

Figure 1. Timeline and surgical procedure of the spina bifida aperta (SBA) model. **(A)** Schematic drawing of the experimental timeline. Induction of the defect and immediate correction was performed on day 23-24 gestation. Terminal caesarean delivery was done on day 30-31 gestation and harvest of the pups were done immediately after birth. **(B)** Five essential steps performed during induction of SBA defect; exteriorization of tails and lower lumbar region, creation of a skin defect at the level of the posterior iliac crest and above, removal of bilateral paraspinal muscles, laminectomy and durectomy. **(C)** Three essential steps performed during immediate correction of the defect; undermining of the skin around the defect, application of dural patch (DuraGen® Plus™ in the picture) over the spinal cord and suture to reapproximate the skin layer. **(D)** At-birth images of the unrepaired SBA lesion and repaired lesion. **(E)** Hindbrain herniation. Note that only the unrepaired SBA group demonstrated hindbrain herniation; the cerebral vermis was extended beyond the Basion-Opisthion reference line). Scale bar: 0.5 cm.

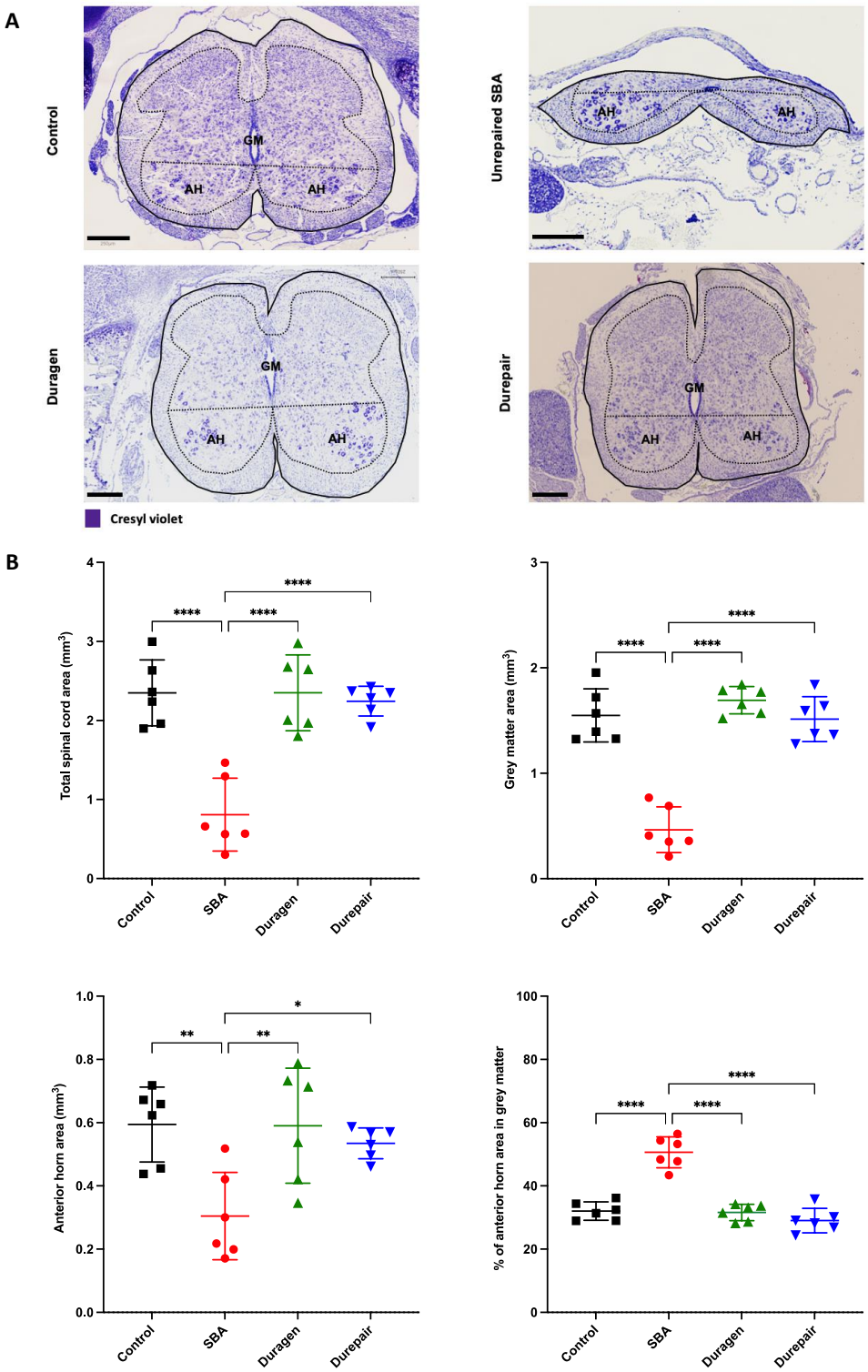

Figure 2. Spinal cord structure of rabbit pups. **(A)** Representative pictures of spinal cord stained with Cresyl violet indicate posterior horn damage in the unrepaired SBA group and well-preserved spinal cord structure in the Duragen and the Durepair groups. **(B)** Total spinal cord area, grey natter area, anterior horn area and % of anterior horn area are significantly smaller in the SBA groups when compared with the control, the Duragen and the Durepair groups. Scale bar: 200 µm. **p<0.05, **p<0.01 , ****p<0.0001.*

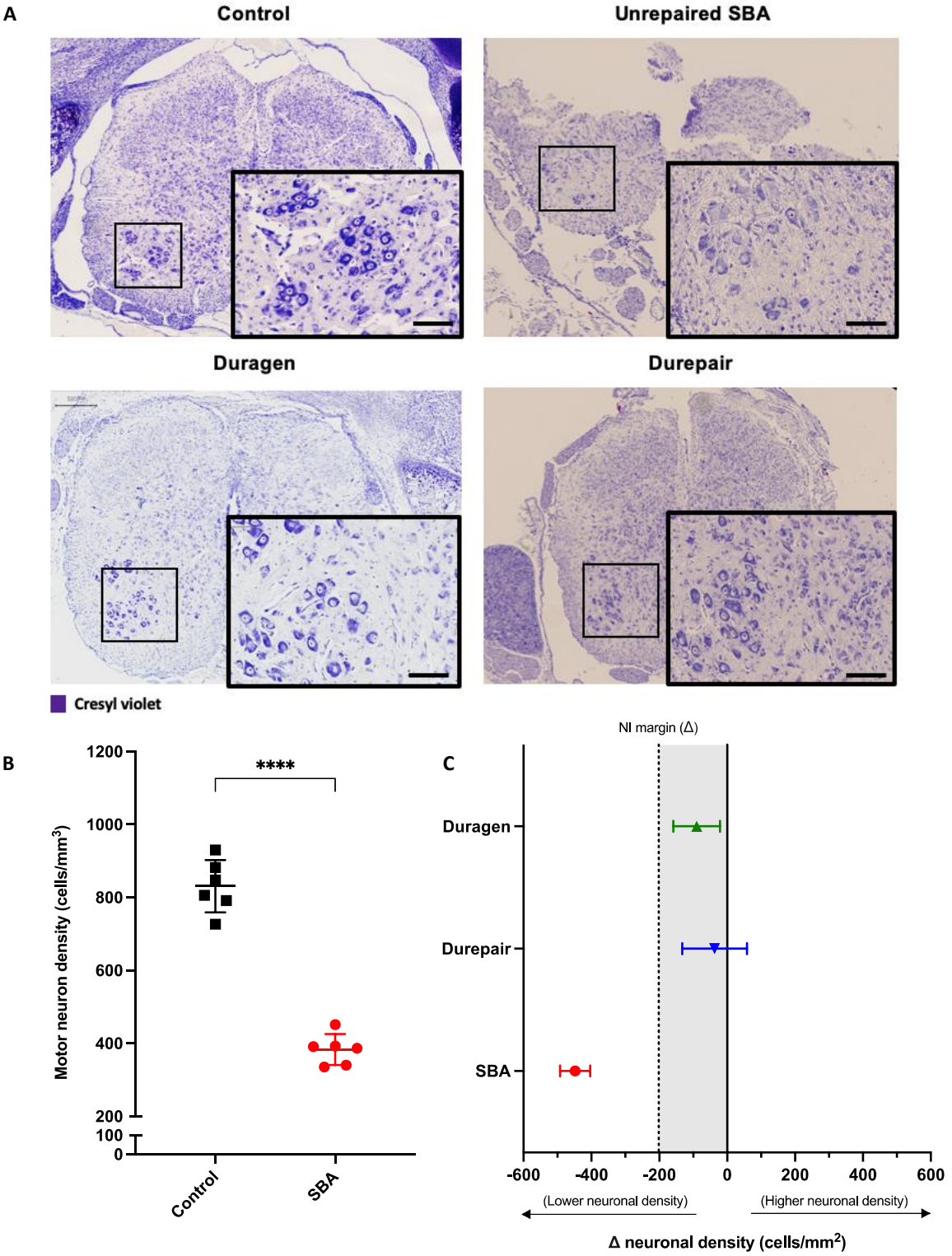

Figure 3. Motor neuron density in the anterior horn of the rabbit pups. **(A)** Representative pictures of spinal cord stained with Cresyl violet indicate a lower density of motor neuron in the anterior horn of the unrepaired SBA group when compared to the other groups. **(B)** Rabbit pups in the unrepaired SBA group has a significantly lower motor neuron density in the anterior horn when compared to the control group. **(C)** Regarding the non-inferiority test between the Duragen/the Durepair and the control group, the motor neuron densities in both the repaired groups were not inferior to those of the control group. Scale bar: 500 µm. *****p<0.0001.*

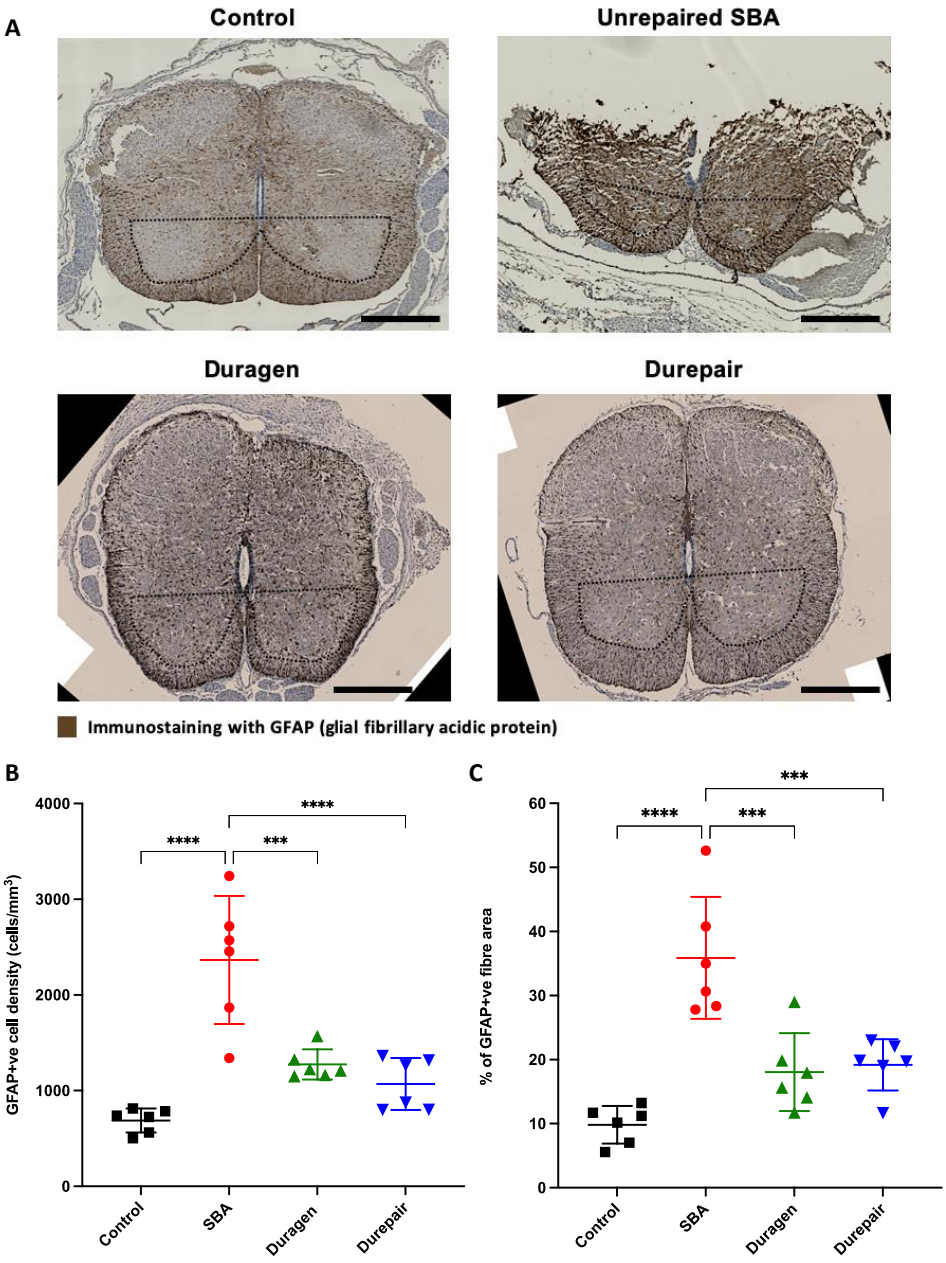

Figure 4. GFAP-positive cell and their fibre densities in the anterior horn of the rabbit pups. **(A)** Representative pictures of spinal cord stained with glial fibrillary acidic protein (GFAP) indicate a higher density of the immunostaining in the anterior horn of the unrepaired SBA group when compared to the other groups. **(B)** Rabbit pups in the unrepaired SBA group has a significantly higher GFAP-positive cell density when compared to the control, Duragen and Durepair groups. **(C)** Rabbit pups in the unrepaired SBA group has a significantly higher GFAP-positive fibre density when compared to the control, Duragen and Durepair groups. Scale bar: 500 µm. *** *p<0.001, ****p<0.0001.*